

Title: **Ultrafast behavior of induced and intrinsic magnetic moments in CoFeB/Pt bilayers probed by element-specific measurements in the extreme ultraviolet spectral range**



Author(s): Clemens von Korff Schmising, Somnath Jana, Kelvin Yao, Martin Hennecke, Philippe Scheid, Sangeeta Sharma, Michel Viret, Jean-Yves Chauleau, Daniel Schick, and Stefan Eisebitt





Document type: Preprint

Terms of Use: Copyright applies. A non-exclusive, non-transferable and limited right to use is granted. This document is intended solely for personal, non-commercial use.

Citation:

"Clemens von Korff Schmising u.a., 2023, Phys. Rev. Research 5, 013147 ; <https://doi.org/10.1103/PhysRevResearch.5.013147>"
Archiviert unter: <http://dx.doi.org/10.17169/refubium-42477>


Ultrafast behavior of induced and intrinsic magnetic moments in CoFeB/Pt bilayers probed by element-specific measurements in the extreme ultraviolet spectral range

Clemens von Korff Schmising ^{1,*}, Somnath Jana,¹ Kelvin Yao,¹ Martin Hennecke ¹, Philippe Scheid,¹ Sangeeta Sharma,¹ Michel Viret,² Jean-Yves Chauleau,² Daniel Schick ¹ and Stefan Eisebitt ^{1,3}

¹Max-Born-Institut für Nichtlineare Optik und Kurzzeitspektroskopie, Max-Born-Straße 2A, 12489 Berlin, Germany

²SPEC, CEA, CNRS, Université Paris-Saclay, CEA Saclay - 91191 Gif sur Yvette, France

³Technische Universität Berlin, Institut für Optik und Atomare Physik, 10623 Berlin, Germany

 (Received 21 October 2022; revised 30 January 2023; accepted 2 February 2023; published 27 February 2023)

The ultrafast and element-specific response of magnetic systems containing ferromagnetic $3d$ transition metals and $4d/5d$ heavy metals is of interest both from a fundamental as well as an applied research perspective. However, to date no consensus about the main microscopic processes describing the interplay between intrinsic $3d$ and induced $4d/5d$ magnetic moments upon femtosecond laser excitation exist. In this work we study the ultrafast response of CoFeB/Pt bilayers by probing element-specific, core-to-valence-band transitions in the extreme ultraviolet spectral range using high harmonic radiation. We show that the combination of magnetic scattering simulations and analysis of the energy- and time-dependent magnetic asymmetries allows us to accurately disentangle the element-specific response in spite of overlapping Co and Fe $M_{2,3}$ as well as Pt $O_{2,3}$ and N_7 resonances. We find a considerably smaller demagnetization time constant as well as much larger demagnetization amplitudes of the induced moment of Pt compared to the intrinsic moment of CoFeB. Our results are in agreement with enhanced spin-flip probabilities due to the high spin-orbit coupling localized at the heavy metal Pt, as well as with the recently formulated hypothesis that a laser-generated, incoherent magnon population within the ferromagnetic film leads to an overproportional reduction of the induced magnetic moment of Pt.

DOI: [10.1103/PhysRevResearch.5.013147](https://doi.org/10.1103/PhysRevResearch.5.013147)

I. INTRODUCTION

Combining ferromagnetic $3d$ transition metals with $4d/5d$ heavy metals leads to magnetic systems with new macroscopic functionalities. Co/Pt multilayers or FePt nanoparticles, for example, exhibit very high magnetocrystalline anisotropies and are therefore important model systems for data storage technology. Pt underlayers can be exploited for spin-orbit-torque-induced switching [1,2] with potential for ultrafast applications [3]. Light-driven processes allowing the manipulation and control of ferromagnetic order are receiving renewed attention due to the discovery of helicity-dependent, all-optical switching in thin Co/Pt multilayers and FePt-based granular films [4], with promising new developments based on tailored double-pulse excitation schemes [5].

The ultrafast response of optically excited ferromagnetic transition metal or heavy metal systems is characterized by their very different atomic spin-orbit coupling strength, their distinct electronic structures, and importantly, by the behavior of intrinsic $3d$ versus induced $4d/5d$ magnetic moments.

The phenomenon of proximity-induced magnetism is caused by hybridization of the $3d$ and $4d/5d$ bands and leads to parallel spin alignment between the intrinsic and induced moments [6,7]. The complex interplay of the involved elements after optical excitation has been studied in a growing number of element-specific experiments based on resonant x-ray or extreme ultraviolet spectroscopy, leading, however, to conflicting observations and corresponding competing theoretical explanations. While experiments with Co/Pt bi- [8] or multi- [9] layers as well as FePt alloys [10] suggest that the induced Pt moment follows the dynamics of the ferromagnetic transition metal, later work found clear evidence for a distinct, element-specific response—both in an ordered FePt compound [11] as well as in a Co/Pt multilayer [12]. There, a significantly slower dynamics of Pt was found and rationalized with a higher mobility of Co or Fe compared to Pt majority electrons, leading to an enhanced demagnetization rate of the transition metal due to superdiffusive spin currents. Additionally, ground-state density-of-state calculations have predicted that a potential generation of incoherent magnons would lead to an overproportional reduction of the induced compared to the intrinsic magnetic moments: as canting of the $3d$ spins changes the average spin alignment between neighboring atoms, the exchange interactions on the $4d/5d$ heavy metal is reduced, leading to a reduction of the induced moment. These calculations showed that if the response of the transition metal is dominated by Heisenberg-like, transversal excitation, the induced moment behaves differently and

*korff@mbi-berlin.de

Published by the American Physical Society under the terms of the [Creative Commons Attribution 4.0 International license](https://creativecommons.org/licenses/by/4.0/). Further distribution of this work must maintain attribution to the author(s) and the published article's title, journal citation, and DOI.

exhibits a strong reduction of its *amplitude* [11,13]. The aforementioned study investigating a CoPt alloy qualitatively confirmed this hypothesis, revealing slightly larger demagnetization amplitudes of Pt compared to Co [13]. An explanation based on enhanced spin-orbit coupling of the heavy metal Pd and a respective stronger spin-flip probability was invoked to rationalize an accelerated demagnetization rate with increasing Pd concentrations in NiPd alloys [14]. Finally, we suggested a scenario where optical intersite spin transfer (OISTR) [15], i.e., a laser-driven transfer of minority carriers from Pt to Co, competes with spin-orbit-driven spin-flips locally enhanced on the Pt atom, resulting in comparable magnetization dynamics of Co and Pt. Experimentally, this hypothesis was tested in an experiment investigating a CoPt alloy using a combination of ultrafast magnetic circular dichroism and helicity-dependent transient absorption spectroscopy in the XUV spectral range [16]. Also based on OISTR, *ab initio* calculations of the ultrafast magnetization changes of a FePd₃ compound predicted element-specific dynamics with a qualitative dependence on the laser pulse intensity [17].

However, when evaluating and comparing these results in literature, it is important to acknowledge the different experimental techniques, different excitation levels and, most importantly, the different studied sample geometries, ranging from alloys with different stoichiometries to bi- and multilayers with different film thicknesses leading to very different local environments. While in reflection geometry with an enhanced surface sensitivity, superdiffusive spin currents may lead to a distinct $3d$ versus $4d/5d$ response [10–13], experiments in transmission geometry yield signals averaged over the entire sample volume and will be less affected by intralayer spin transport [8,9,16]. OISTR is confined to spin transfer among nearest neighbors [18,19] and is hence expected to be most pronounced in alloys with equal concentrations of Co and Pt or ultrathin layered systems.

In this study we report on distinct, layer-dependent dynamics of a CoFeB(5.3 nm)/Pt(3.5 nm) bilayer observed by element-specific, transverse magneto-optical Kerr effect (T-MOKE) measurements in the XUV spectral range using radiation of a high harmonic generation (HHG) source. We demonstrate that the combination of magnetic scattering simulations [20,21] and an analysis of the ultrafast response at different photon energies allows accurately separating the element-specific response of Co or Fe and Pt in spite of strongly overlapping resonances. The experimental results reveal a transient magnetic state with a significantly faster and more efficient quenching of the induced Pt moments compared to the response of the transition-metal CoFeB alloy. A systematic comparison with a CoFeB/MgO/Pt system, exhibiting no induced magnetization of Pt, supports our analysis.

II. EXPERIMENT

Si/Co₄₀Fe₄₀B₂₀(5.3 nm)/MgO(1 nm)/Pt(3.5 nm) as well as Si/Co₄₀Fe₄₀B₂₀(5.3 nm)/Pt(3.5 nm) were deposited on Si substrates by magnetron sputtering. Both samples exhibit an in-plane magnetization and a square hysteresis loop with a small coercive field below 2 mT. The magnetic films are protected against oxidation by the Pt layer or MgO/Pt bilayer.

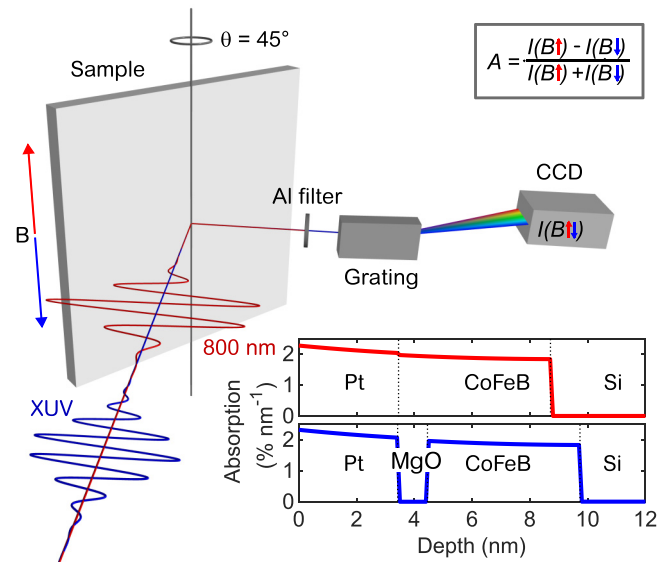


FIG. 1. Schematic of the T-MOKE geometry with an incident angle $\theta = 45^\circ$ of the p -polarized XUV radiation. After reflection, the XUV pulses are spectrally dispersed by a flat field concave grating and detected by a CCD camera. An external magnetic field B is aligned perpendicularly to the incoming p -polarized XUV light. The sample is excited by laser pulses at $\lambda = 800$ nm in a nearly collinear geometry. The inset shows the depth-dependent absorption profiles of the CoFeB/Pt and CoFeB/MgO/Pt samples.

The thicknesses as well as interface roughnesses of below 0.5 nm have been confirmed by independent x-ray reflectivity measurements.

A schematic of the setup is shown in Fig. 1. Intense laser pulses at a repetition rate of 3 kHz, a central wavelength of $\lambda = 800$ nm and a pulse length of 25 fs are focused into a cell filled with neon gas, leading to higher harmonic radiation. The emitted XUV spectrum consists of discrete peaks with an approximate spectral width of 200 meV. Additionally, we generate continuous spectra for the static characterization by averaging multiple acquisitions with varied chirp and peak intensities of the laser pulses, as well as with varying gas pressures. The p -polarized XUV radiation is incident on the sample at an angle of $\theta = 45^\circ$, reflected, and then spectrally dispersed by a flat field concave grating and detected by a charged coupled device (CCD). The magnetization of the sample is set by applying an external magnetic field perpendicular to the incident polarization, facilitating the T-MOKE geometry [22]. The magnetic asymmetry A is calculated as the normalized difference of two spectra I , recorded for opposite magnetization directions of the CoFeB film, cf. Fig. 1. The time-resolved experiments were performed in a pump-probe geometry using pump pulses with a central wavelength of 800 nm and a pulse duration of <30 fs as confirmed by auto-correlation measurements at the sample position. We estimate the upper bound for the temporal resolution of the experiment to be 35 fs. The absolute values of incident fluences between 0 and 12 mJcm⁻² are determined by a calibrated power meter and careful measurements of the beam area (full width at half maximum) using a beam profile camera. Calculations of the layer-dependent absorption profile based on a multilayer

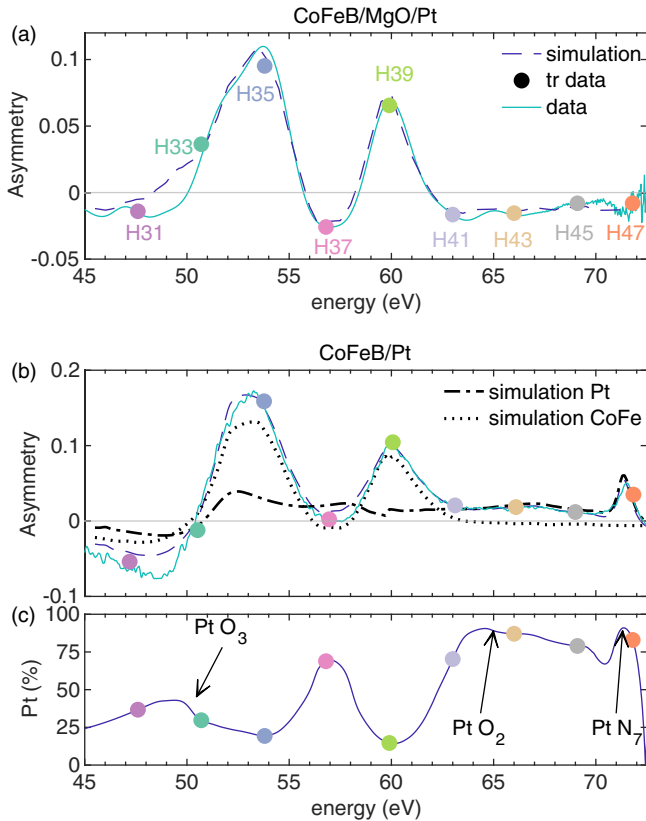


FIG. 2. Measured and calculated static magnetic asymmetry of (a) CoFeB/MgO/Pt and (b) CoFeB/Pt as a function of photon energy. The color-coded dots mark the photon energies of the time-resolved measurements, while the solid lines are static measurements with a continuous HHG spectrum. In (b) we additionally show the calculated magnetic asymmetry stemming from CoFe (dotted line) and Pt (dashed line). The largest relative contributions to the magnetic asymmetry of Pt are not only found around the Pt $O_{2,3}$ and Pt N_7 edges, but also at 57 eV, where contribution of Co and Fe approaches zero, cf. panel (c).

formalism [20,21], using literature values of the optical refractive indices [23,24], show an almost homogeneous energy deposition within the CoFeB and Pt layers (cf. Fig. 1). To improve the signal-to-noise ratio, we acquire the incoming spectrum with a separate spectrometer for normalization and repeat each time-delay scan up to 50 times. For more details on the experimental setup, please refer to Yao *et al.* [25].

III. RESULTS

In Fig. 2 we show the magnetic asymmetry in a photon energy range between 45 and 72.5 eV for both samples, (a) CoFeB/MgO/Pt and (b) CoFeB/Pt. We plot the asymmetry measured with a continuous HHG spectrum and mark the photon energies of the nine discrete HHG peaks (H31–H47) used in the time-resolved experiments with colored dots. The simulations for static asymmetries are carried out with the `udkm1Dsim` toolbox [20,21] numerically calculating the polarization-dependent wave propagation, taking into account refraction and reflections of the nanolayered systems. We use published values of the atomic and magnetic form factors of

Fe and Co [26] and extract values for the induced moment of Pt from measurements of CoPt [8,27]. Atomic form factors of MgO and B are taken from Henke *et al.* [28]. We keep the thicknesses and interface roughnesses fixed but allow small variations in the densities as well as in the absolute values of the elemental magnetic moments. For the CoFeB/Pt system, we fix the thickness of the magnetized Pt layer at the interface to 1 nm [7,29,30]. The fitting results yield a good agreement with the experimental measurements; for both samples we can clearly note the dominant contributions from the Fe and Co $M_{2,3}$ edges around 53.5 eV and 60 eV probed by the HHG emission peaks H35 and H39. In the energy range between 47 eV and 51 eV, both samples exhibit qualitatively similar deviations between simulation and experiment. As in the CoFeB/MgO/Pt sample Pt is not magnetic, we can rule out that they are caused by incorrect magnetic form factors of Pt. For CoFeB/Pt the simulation also slightly overestimates the small magnetic asymmetries around 57 eV, probed by HHG peak H37. For the CoFeB/Pt sample, we extract the contributions of Pt to the magnetic asymmetry by setting the magnetic moment of Co and Fe to zero. This is shown as a dashed-dotted line in Fig. 2(b). The contribution of the CoFeB layer is calculated accordingly and shown as a dotted line. While this approach neglects the influence of the dichroic part of the refractive index of either Pt and Co or Fe to the reflectivities, we validate this approximation by finding an excellent agreement between the sum of the individual asymmetries and the total asymmetry of CoFeB/Pt. In Fig. 2(c) we plot the relative contribution of Pt to the magnetic asymmetry of the CoFeB/Pt sample, which is determined by the complex spectral overlap of the three magnetic elements Co, Fe, and Pt. The asymmetry of harmonic H35 is dominated by Fe (80%), and H39 is dominated by Co (85%). The maximum relative contribution of Pt is at the Pt N_7 edge at 71.2 eV with close to 90%. The small asymmetries beyond the Co edge (harmonic peaks H41–H45) are also dominated by Pt and yield values $>80\%$. Furthermore, the harmonic peak H33 and H37 exhibit appreciable Pt $O_{2,3}$ contributions of 30% and 70%. The system CoFeB/MgO/Pt is not expected to exhibit a static induced magnetization of Pt, which, within our signal-to-noise ratio, is also consistent with our simulation. The subtle differences of the energy-dependent magnetic asymmetries between both sample systems highlights the importance of dedicated calculations in order to extract element-specific information in the XUV spectral range.

A summary of time-resolved data is shown in Fig. 3 for very early times after optical excitation. We plot data for two exemplary fluences: 10 mJcm^{-2} and 4 mJcm^{-2} for the samples CoFeB/Pt and CoFeB/MgO/Pt, respectively. The solid lines are fits using a single exponential decay convolved with a Gauss function $G(t)$, reflecting the temporal resolution of the experiment:

$$A(t) = G(t) * [A_0 + \Theta(t)(B(e^{-t/\tau} - 1))], \quad (1)$$

where $\Theta(t)$ is the Heaviside function, A_0 is the static asymmetry, B the amplitude of the demagnetization, and τ denotes the demagnetization time constant. We differentiate the ultrafast response of the CoFeB/Pt sample measured at the different harmonics according to their element specificity: H35 and H39 are dominated by Fe and Co,

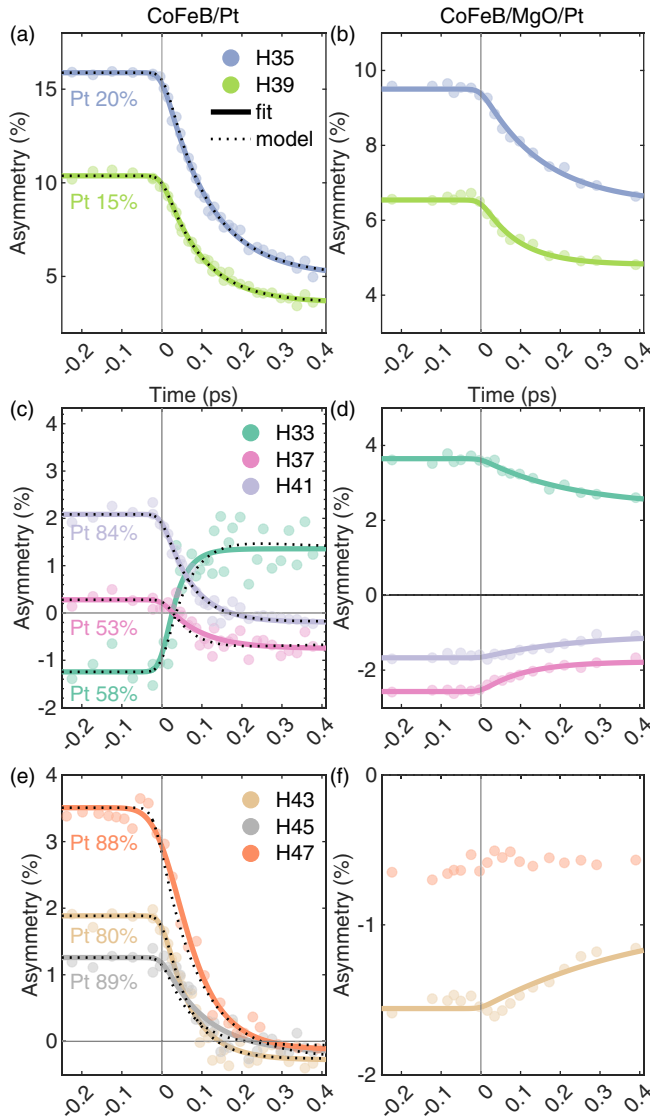


FIG. 3. Magnetic asymmetry as a function of time after optical excitation. Harmonics H35 and H39 in panel (a) and (b) are dominated by the dynamics of Fe and Co, respectively. For the CoFeB/Pt system, HHG peaks H33 and H37 [panel (c)] are sensitive to both layers, CoFeB and Pt, and are characterized by a sign change of the time-resolved asymmetry. The asymmetries of the HHG peaks H41 [panel (c)], H43, H45, and H47 [panel (a)] are dominated by Pt contributions and, different from H35 and H39, exhibit a 100% reduction of A . For the CoFeB/MgO/Pt sample system, all shown harmonics H33–H47 show the same relative demagnetization amplitude and represent the response of Fe or Co. Harmonic H47, close to the Pt N_7 edge, shows no evidence of an increase, i.e., no evidence for tunneling of spin-polarized carriers from the CoFeB to Pt via the MgO layer, cf. panel (f).

respectively, and are shown in panel (a); H33, H37, and H41 display a significant admixture with Pt and are summarized in panel (c); and finally, H43, H45, and H47 predominately reflect the ultrafast dynamics of Pt and are shown in panel (e). The response of the CoFeB/MgO/Pt sample at corresponding photon energies is shown in panels (b), (d), and (f). For the CoFeB/Pt sample, we find demagnetization time constants

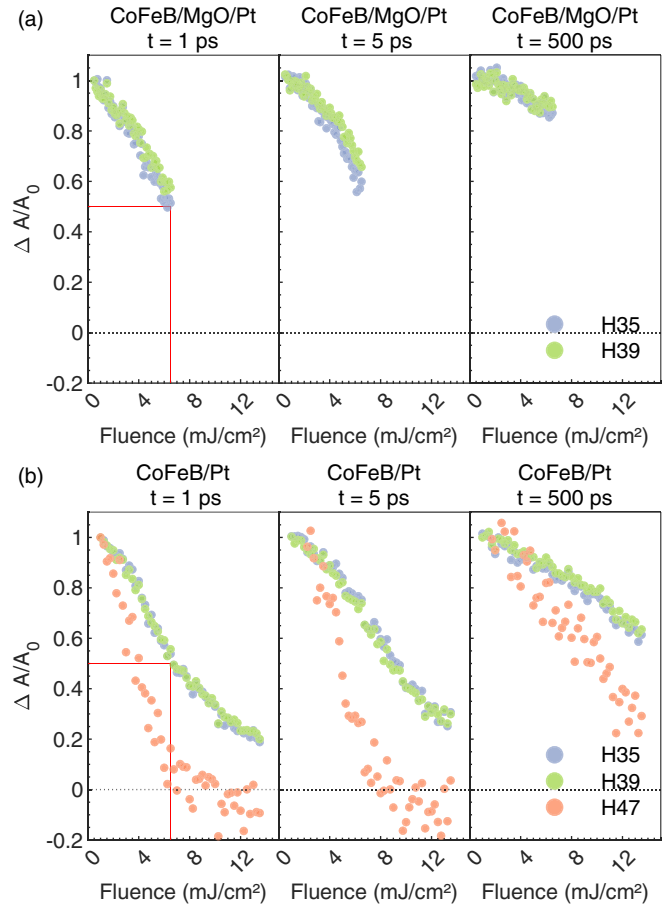


FIG. 4. Normalized asymmetry $\Delta A/A_0$ as a function of excitation fluence for three selected time delays, $t = 1, 5, 500$ ps. In panel (a) we show H35 (Fe) and H39 (Co) for the CoFeB/MgO/Pt and in (b) additionally H47 (Pt) for the CoFeB/Pt system. Pt demagnetizes significantly more efficiently and remains out of equilibrium with the CoFeB layer for up to 500 ps.

for H35 $\tau_{H35} = (115 \pm 7)$ fs and for H39 $\tau_{H39} = (105 \pm 6)$ fs; for the CoFeB/MgO/Pt sample the values amount to $\tau_{H35} = (140 \pm 20)$ fs and $\tau_{H39} = (100 \pm 19)$ fs. Within our signal-to-noise ratio, we do not find any systematic variations of the demagnetization constants, neither for the two different samples nor as a function of fluence. However, the slightly faster demagnetization constant of H39 (Co) compared to H35 (Fe) is consistently reproduced and is also in agreement with previous observations that τ scales with the magnetic moment of the element [31,32]. The average of the extracted demagnetization time constants of harmonics H41–H47 amounts to $\tau_{H41-H47} = (70 \pm 20)$ fs, significantly smaller than what we find for H35 (Fe) and H39 (Co). Furthermore, the magnetic asymmetries measured for CoFeB/Pt at photon energies dominated by Pt, i.e., H41, H43, H45, and H47 shown in Figs. 3(c) and 3(e) are completely quenched or even show small negative values at $t = 400$ fs. This is in contrast to asymmetry values of harmonics H35 and H39, which are only reduced by 35% at this time delay.

The demagnetization amplitudes for different photon energies are more easily compared by inspection of Fig. 4, where we display the normalized magnetic asymmetries, $\hat{A} =$

$\Delta A/A_0$, as a function of the incident fluence at three selected time delays of $t = 1, 5,$ and 500 ps. Data for harmonics H35 and H39 show very similar values over the entire fluence range and for the three different times. This also applies for both sample systems: the red lines mark $\Delta A(t = 1\text{ps})/A_0 = 0.5$, which is reached for an incident fluence of 6.5mJcm^{-2} for both samples. In Fig. 4(b) we additionally show the magnetic asymmetry of harmonic H47 measured for sample CoFeB/Pt. Clearly, here $\Delta A/A_0$ is reduced more efficiently and already reaches zero for a fluence of $\approx 8\text{mJcm}^{-2}$. Also note that even after a time delay of 500 ps, when the CoFeB layer has recovered a significant fraction of its magnetization by energy dissipation, the magnetization of the Pt layer remains out of equilibrium with CoFeB. With the assignment of the different harmonic peaks to the different magnetic elements within the sample, this presents strong evidence that the interfacial Pt layer loses its induced magnetization significantly more efficiently than Co and Fe.

The element-specific dynamics allows us to use the time-resolved data to further verify and refine the relative elemental contributions to the magnetic asymmetry discussed in Fig. 2(c). Accordingly, we describe the normalized nonlinear least-square fits of the data (solid lines in Fig. 3) by a sum of Eq. (1) representing separately the response of Co/Fe and Pt:

$$\hat{A}(t) = c_{\text{Pt}}\hat{A}_{\text{Pt}}(t) + c_{\text{Co/Fe}}\hat{A}_{\text{Co/Fe}}(t). \quad (2)$$

We use the extracted demagnetization time constants measured for H35, H39 as well as the average of H41–H47 and assign them to Co, Fe, and Pt, respectively. The normalized demagnetization amplitude \hat{B} of Pt is assumed to be 100%. We then describe our normalized, time-dependent data $\hat{A}(t)$ by Eq. (2) and only treat the demagnetization amplitude \hat{B} of Co or Fe as well as the relative weights c_{Pt} and $c_{\text{Co/Fe}}$ as free parameters. Additionally, the following condition has to hold: $c_{\text{Pt}} + c_{\text{Co/Fe}} = 1$. The results are shown as dotted lines in Figs. 3(a), 3(c) and 3(e). Analysis of the response of H35 and H39 yield demagnetization amplitudes for Fe and Co of $(40 \pm 5)\%$. The extracted relative Pt contributions are shown next to the time-resolved transients. We find a good agreement with the values determined from the static simulation, except for H33 and H37, where we see a substantial deviation. We attribute this to the very low values of the absolute asymmetry values in this energy range. A remarkable feature of the time traces of H33 and H37 is the sign change of the asymmetry. This is caused by the opposite sign of the respective asymmetries as well as the very different ultrafast response of the FeCoB and Pt layers. As Pt completely demagnetizes and CoFeB does not, the asymmetries reverse sign, which is quantitatively reproduced by Eq. (2). The same argument holds for photon energies H43–H47, where we also observe a zero crossing of A . Importantly, the observed sign change of the asymmetry is not related to a magnetization reversal. Another potential explanation for the sign change of A of H33 and H37 could be related to a spectral reshaping of A , as these photon energies probe the system very close to a zero crossing of the static asymmetry spectra. Such spectral reshaping, effectively shifting the resonant absorption and circular dichroism to smaller energies, has been recently postulated for the XUV spectral range and is understood to be caused by laser-driven changes of electron occupations [33–35]. However, as the

slopes of A at energies H33 and H37 are very different, a laser-induced spectral shift would result in significantly different dynamic changes, which is contrary to our observation. Combining the static and time-resolved analysis, we estimate the uncertainty in assigning the relative elemental contribution for HHG peaks H33 and H37 of up to 15%, for all other peaks to $<5\%$.

A closer inspection of the ultrafast response of CoFeB/MgO/Pt in Figs. 3(b), 3(d) and 3(f) reveals comparable ultrafast dynamics with demagnetization amplitudes of $\Delta A/A_0 = (30 \pm 5)\%$ at $t = 0.4$ ps for all HHG peaks. The magnetic asymmetry measured at the HHG peak H47, probing the Pt N_7 edge, does not show any evidence of a magnetization increase but stays constant within our signal-to-noise ratio. This implies that we can exclude significant ultrafast spin tunneling through the MgO barrier into Pt, in agreement with a very recent study that found an exponential decay length of only 2\AA for the tunneling spin current through MgO [36]. Just as for the CoFeB/Pt system, we observe similar demagnetization amplitudes of Fe and Co for longer timescales [cf. Fig. 4(a)], pointing towards an identical temperature dependence of the equilibrium magnetization of Co and Fe. This differs from previous observations on $\text{Co}_{60}\text{Fe}_{20}\text{B}_{20}/\text{SiO}_2$ systems, where a difference in the asymptotic limit of the remagnetization process was observed [10].

IV. DISCUSSION AND CONCLUSIONS

Our observations of distinct ultrafast dynamics of *intrinsic* vs *induced* moments can be reconciled with our earlier work on $\text{Co}_{50}\text{Pt}_{50}$ alloys, where we identified two competing processes: spin-orbit-induced spin-flips and OISTR [26]. We argue again that the more efficient demagnetization of Pt may be a consequence of the significantly stronger spin-orbit coupling localized at the Pt atoms compared to Co or Fe [37,38]. At the same time, with fewer Co or Fe-Pt nearest neighbors in the studied bilayer, competing OISTR processes are less likely to occur than in an alloy, leading to distinct dynamics between Co or Fe and Pt in this work.

Qualitatively, our results of a larger demagnetization amplitude of the Pt layer may also support the hypothesis that the induced moment of Pt is very sensitive to the orientation of the intrinsic CoFe moments and could hence be interpreted as an indicator for the generation of incoherent magnons in the CoFeB layer. In Yamamoto *et al.* [11], however, it was postulated that magnons are predominantly generated after relaxation of the nonequilibrium electron distribution and will therefore only start to dominate after ≈ 1 ps, i.e., on a slower timescale compared to our observations. On the other hand, a number of recent studies have found evidence for an ultrafast generation of incoherent magnons upon laser excitation [39–44]. Also, our observation that the magnetization of the Pt layers remains out of equilibrium with the adjacent CoFeB layer for delays larger than 500 ps, i.e., much longer than heat equilibration times, may count as a further indication that induced moments of Pt are very sensitive to long-lived magnon populations of the polarizing Co or Fe moments. We anticipate that the combination of time-dependent density-of-

state calculations with experiments reaching a significantly improved temporal resolution may be able to disentangle the different processes in the time domain and identify the timescale on which such a potential magnon population emerges.

Our results do not show any clear signatures of superdiffusive spin currents, in spite of also using a reflection geometry with depth-dependent sensitivity [45]. A potential interlayer spin transport would be characterized by injection of majority carriers from CoFeB to the interface region of the Pt layer, leading to an increase of the demagnetization rate of the CoFeB layer while simultaneously decreasing the demagnetization rate in the Pt layer, which is different to our observation. Also, the almost identical demagnetization rate of the CoFeB/Pt and CoFeB/MgO/Pt system (cf. red lines in Fig. 4) rules out significant interlayer superdiffusive spin currents, as transport would be inhibited in the latter sample by the insulating MgO layer.

In conclusion, we have presented a systematic comparison of two sample systems with and without an induced magnetization of Pt, CoFeB/Pt, and CoFeB/MgO/Pt, and demonstrated that a combination of calculated magnetic

asymmetries taking into account the geometry of the sample structure and an analysis of time-resolved magnetization traces allows us to accurately disentangle the element-specific magnetic response in spite of strongly overlapping Co or Fe $M_{2,3}$ and Pt $O_{2,3}$ as well as N_7 resonances. We find a significantly more efficient demagnetization rate of the induced moment of Pt compared to the intrinsic moment of the transition metals in a CoFeB/Pt bilayer. Our results are in agreement with the presence of enhanced spin-orbit-driven spin-flips localized on Pt, as well as with the recently postulated hypothesis of a strong sensitivity of an induced $4d/5d$ magnetic moment to the potential ultrafast emergence of an incoherent magnon population.

ACKNOWLEDGMENTS

C.v.K.S., S.S., and S.E. acknowledge financial support by the Deutsche Forschungsgemeinschaft (DFG, German Research Foundation) through Project ID Nos. 328545488 - TRR 227, A02, and A04. J.-Y.C. acknowledges funding from the French National Research Agency ANR JCJC through the SPINUP project, Ref. No. ANR-21-CE24-0026-01.

-
- [1] A. Brataas, A. D. Kent, and H. Ohno, Current-induced torques in magnetic materials, *Nat. Mater.* **11**, 372 (2012).
- [2] B. Dieny, I. L. Prejbeanu, K. Garello, P. Gambardella, P. Freitas, R. Lehdorff, W. Raberg, U. Ebels, S. O. Demokritov, J. Akerman, A. Deac, P. Pirro, C. Adelman, A. Anane, A. V. Chumak, A. Hirohata, S. Mangin, S. O. Valenzuela, M. C. Onbaşlı, M. d'Aquino *et al.*, Opportunities and challenges for spintronics in the microelectronics industry, *Nat. Electron.* **3**, 446 (2020).
- [3] K. Jhuria, J. Hohlfield, A. Pattabi, E. Martin, A. Y. A. Córdova, X. Shi, R. L. Conte, S. Petit-Watelot, J. C. Rojas-Sanchez, G. Malinowski, S. Mangin, A. Lemaître, M. Hehn, J. Bokor, R. B. Wilson, and J. Gorchon, Spin-orbit torque switching of a ferromagnet with picosecond electrical pulses, *Nat. Electron.* **3**, 680 (2020).
- [4] C.-H. Lambert, S. Mangin, B. S. D. C. S. Varaprasad, Y. K. Takahashi, M. Hehn, M. Cinchetti, G. Malinowski, K. Hono, Y. Fainman, M. Aeschlimann, and E. E. Fullerton, All-optical control of ferromagnetic thin films and nanostructures, *Science* **345**, 1337 (2014).
- [5] K. T. Yamada, A. V. Kimel, K. H. Prabhakara, S. Ruta, T. Li, F. Ando, S. Semin, T. Ono, A. Kirilyuk, and T. Rasing, Efficient all-optical helicity dependent switching of spins in a Pt/Co/Pt film by a dual-pulse excitation, *Front. Nanotechnol.* **4**, 765848 (2022).
- [6] F. Hellman, A. Hoffmann, Y. Tserkovnyak, G. S. D. Beach, E. E. Fullerton, C. Leighton, A. H. MacDonald, D. C. Ralph, D. A. Arena, H. A. Dürr, P. Fischer, J. Grollier, J. P. Heremans, T. Jungwirth, A. V. Kimel, B. Koopmans, I. N. Krivorotov, S. J. May, A. K. Petford-Long, J. M. Rondinelli *et al.*, Interface-induced phenomena in magnetism, *Rev. Mod. Phys.* **89**, 025006 (2017).
- [7] N. Nakajima, T. Koide, T. Shidara, H. Miyauchi, H. Fukutani, A. Fujimori, K. Iio, T. Katayama, M. Nývlt, and Y. Suzuki, Perpendicular Magnetic Anisotropy Caused by Interfacial Hybridization via Enhanced Orbital Moment in Co/Pt Multilayers: Magnetic Circular X-Ray Dichroism Study, *Phys. Rev. Lett.* **81**, 5229 (1998).
- [8] F. Willems, C. T. L. Smeenk, N. Zhavoronkov, O. Kornilov, I. Radu, M. Schmidbauer, M. Hanke, C. von Korff Schmising, M. J. J. Vrakking, and S. Eisebitt, Probing ultrafast spin dynamics with high-harmonic magnetic circular dichroism spectroscopy, *Phys. Rev. B* **92**, 220405(R) (2015).
- [9] M. Hennes, G. Lambert, V. Chardonnet, R. Delaunay, G. S. Chiuzbăian, E. Jal, and B. Vodungbo, Element-selective analysis of ultrafast demagnetization in Co/Pt multilayers exhibiting large perpendicular magnetic anisotropy, *Appl. Phys. Lett.* **120**, 072408 (2022).
- [10] M. Hofherr, S. Moretti, J. Shim, S. Häuser, N. Y. Safonova, M. Stiehl, A. Ali, S. Sakshath, J. W. Kim, D. H. Kim, H. J. Kim, J. I. Hong, H. C. Kapteyn, M. M. Murnane, M. Cinchetti, D. Steil, S. Mathias, B. Stadtmüller, M. Albrecht, D. E. Kim *et al.*, Induced versus intrinsic magnetic moments in ultrafast magnetization dynamics, *Phys. Rev. B* **98**, 174419(R) (2018).
- [11] K. Yamamoto, Y. Kubota, M. Suzuki, Y. Hirata, K. Carva, M. Berritta, K. Takubo, Y. Uemura, R. Fukaya, K. Tanaka, W. Nishimura, T. Ohkochi, T. Katayama, T. Togashi, K. Tamasaku, M. Yabashi, Y. Tanaka, T. Seki, K. Takashi *et al.*, Ultrafast demagnetization of Pt magnetic moment in L_{10} -FePt probed by magnetic circular dichroism at a hard x-ray free electron laser, *New J. Phys.* **21**, 123010 (2019).
- [12] K. Yamamoto, S. E. Moussaoui, Y. Hirata, S. Yamamoto, Y. Kubota, S. Owada, M. Yabashi, T. Seki, K. Takashi, I. Matsuda, and H. Wadati, Element-selectively tracking ultrafast demagnetization process in Co/Pt multilayer thin films by the resonant magneto-optical Kerr effect, *Appl. Phys. Lett.* **116**, 172406 (2020).
- [13] I. Vaskivskiy, R. S. Malik, L. Salemi, D. Turenne, R. Knut, J. Brock, R. Stefanuik, J. Söderström, K. Carva, E. E. Fullerton,

- P. M. Oppeneer, O. Karis, and H. A. Dürr, Element-specific magnetization dynamics in Co-Pt alloys induced by strong optical excitation, *J. Phys. Chem. C* **125**, 11714 (2021).
- [14] S.-g. Gang, R. Adam, M. Plötzing, M. von Witzleben, C. Weier, U. Parlak, D. E. Bürgler, C. M. Schneider, J. Ruzs, P. Maldonado, and P. M. Oppeneer, Element-selective investigation of femtosecond spin dynamics in NiPd magnetic alloys using extreme ultraviolet radiation, *Phys. Rev. B* **97**, 064412 (2018).
- [15] J. K. Dewhurst, P. Elliott, S. Shallcross, E. K. U. Gross, and S. Sharma, Laser-induced intersite spin transfer, *Nano Lett.* **18**, 1842 (2018).
- [16] F. Willems, C. von Korff Schmising, C. Strüber, D. Schick, D. W. Engel, J. K. Dewhurst, P. Elliott, S. Sharma, and S. Eisebitt, Optical inter-site spin transfer probed by energy and spin-resolved transient absorption spectroscopy, *Nat. Commun.* **11**, 871 (2020).
- [17] M. F. Elhanoty, O. Eriksson, R. Knut, O. Karis, and O. Grånäs, Element-selective ultrafast magnetization dynamics of hybrid Stoner-Heisenberg magnets, *Phys. Rev. B* **105**, L100401 (2022).
- [18] J. K. Dewhurst, S. Shallcross, E. K. Gross, and S. Sharma, Substrate-Controlled Ultrafast Spin Injection and Demagnetization, *Phys. Rev. Appl.* **10**, 044065 (2018).
- [19] J. Chen, U. Bovensiepen, A. Eschenlohr, T. Müller, P. Elliott, E. Gross, J. Dewhurst, and S. Sharma, Competing Spin Transfer and Dissipation at Co/Cu(001) Interfaces on Femtosecond Timescales, *Phys. Rev. Lett.* **122**, 067202 (2019).
- [20] D. Schick, A. Bojahr, M. Herzog, R. Shayduk, C. von Korff Schmising, and M. Bargheer, udkm1Dsim—A simulation toolkit for 1D ultrafast dynamics in condensed matter, *Comput. Phys. Commun.* **185**, 651 (2014).
- [21] D. Schick, UDKM1DSIM—A Python toolbox for simulating 1D ultrafast dynamics in condensed matter, *Comput. Phys. Commun.* **266**, 108031 (2021).
- [22] C. La-O-Vorakiat, E. Turgut, C. A. Teale, H. C. Kapteyn, M. M. Murnane, S. Mathias, M. Aeschlimann, C. M. Schneider, J. M. Shaw, H. T. Nembach, and T. J. Silva, Ultrafast Demagnetization Measurements Using Extreme Ultraviolet Light: Comparison of Electronic and Magnetic Contributions, *Phys. Rev. X* **2**, 011005 (2012).
- [23] G.-M. Choi, R. B. Wilson, and D. G. Cahill, Indirect heating of Pt and by short-pulse laser irradiation of Au and in a nanoscale Pt/Au and bilayer, *Phys. Rev. B* **89**, 064307 (2014).
- [24] M. A. Hoffmann, A. Sharma, P. Matthes, S. Okano, O. Hellwig, R. Ecke, D. R. T. Zahn, G. Salvan, and S. E. Schulz, Spectroscopic ellipsometry and magneto-optical Kerr effect spectroscopy study of thermally treated Co₆₀Fe₂₀B₂₀ thin films, *J. Phys.: Condens. Matter* **32**, 055702 (2020).
- [25] K. Yao, F. Willems, C. von Korff Schmising, C. Strüber, P. Hessian, B. Pfau, D. Schick, D. Engel, K. Gerlinger, M. Schneider, and S. Eisebitt, A tabletop setup for ultrafast helicity-dependent and element-specific absorption spectroscopy and scattering in the extreme ultraviolet spectral range, *Rev. Sci. Instrum.* **91**, 093001 (2020).
- [26] F. Willems, S. Sharma, C. v. Korff Schmising, J. K. Dewhurst, L. Salemi, D. Schick, P. Hessian, C. Strüber, W. D. Engel, and S. Eisebitt, Magneto-Optical Functions at the 3P Resonances of Fe, Co, and Ni: Ab Initio Description and Experiment, *Phys. Rev. Lett.* **122**, 217202 (2019).
- [27] J. K. Dewhurst, F. Willems, P. Elliott, Q. Z. Li, C. V. K. Schmising, C. Strüber, D. W. Engel, S. Eisebitt, and S. Sharma, Element Specificity of Transient Extreme Ultraviolet Magnetic Dichroism, *Phys. Rev. Lett.* **124**, 077203 (2020).
- [28] B. Henke, E. Gullikson, and J. Davis, X-ray interactions: Photoabsorption, scattering, transmission, and reflection at E = 50–30,000 eV, Z = 1–92, *At. Data Nucl. Data Tables* **54**, 181 (1993).
- [29] J. Geissler, E. Goering, M. Justen, F. Weigand, G. Schütz, J. Langer, D. Schmitz, H. Maletta, and R. Mattheis, Pt magnetization profile in a Pt/Co bilayer studied by resonant magnetic x-ray reflectometry, *Phys. Rev. B* **65**, 020405(R) (2001).
- [30] M. Suzuki, H. Muraoka, Y. Inaba, H. Miyagawa, N. Kawamura, T. Shimatsu, H. Maruyama, N. Ishimatsu, Y. Isohama, and Y. Sonobe, Depth profile of spin and orbital magnetic moments in a subnanometer Pt film on Co, *Phys. Rev. B* **72**, 054430 (2005).
- [31] B. Koopmans, G. Malinowski, F. Dalla Longa, D. Steiauf, M. Fähnle, T. Roth, M. Cinchetti, and M. Aeschlimann, Explaining the paradoxical diversity of ultrafast laser-induced demagnetization, *Nat. Mater.* **9**, 259 (2010).
- [32] I. Radu, C. Stamm, A. Eschenlohr, F. Radu, R. Abrudan, K. Vahaplar, T. Kachel, N. Pontius, R. Mitzner, K. Hollmack, A. Föhlisch, T. A. Ostler, J. H. Mentink, R. F. Evans, R. W. Chantrell, A. Tsukamoto, A. Itoh, A. Kirilyuk, A. V. Kimel, and T. Rasing, Ultrafast and distinct spin dynamics in magnetic alloys, *Spin* **05**, 1550004 (2015).
- [33] K. Carva, D. Legut, and P. M. Oppeneer, Influence of laser-excited electron distributions on the x-ray magnetic circular dichroism spectra: Implications for femtosecond demagnetization in Ni, *Europhys. Lett.* **86**, 57002 (2009).
- [34] K. Yao, F. Willems, C. von Korff Schmising, I. Radu, C. Strüber, D. Schick, D. Engel, A. Tsukamoto, J. K. Dewhurst, S. Sharma, and S. Eisebitt, Distinct spectral response in M-edge magnetic circular dichroism, *Phys. Rev. B* **102**, 100405(R) (2020).
- [35] B. Rösner, B. Vodungbo, V. Chardonnet, F. Döring, V. A. Guzenko, M. Hennes, A. Kleibert, M. Lebugle, J. Lüning, N. Mahne, A. Merhe, D. Naumenko, I. P. Nikolov, I. Lopez-Quintas, E. Pedersoli, P. R. Ribič, T. Savchenko, B. Watts, M. Zangrando, F. Capotondi, *ibid.*, Simultaneous two-color snapshot view on ultrafast charge and spin dynamics in a Fe-Cu-Ni tri-layer, *Struct. Dyn.* **7**, 054302 (2020).
- [36] M. A. Wahada, E. Şaişoğlu, W. Hoppe, X. Zhou, H. Deniz, R. Rouzegar, T. Kampfrath, I. Mertig, S. S. P. Parkin, and G. Woltersdorf, Atomic scale control of spin current transmission at interfaces, *Nano Lett.* **22**, 3539 (2022).
- [37] K. C. Kuiper, T. Roth, A. J. Schellekens, O. Schmitt, B. Koopmans, M. Cinchetti, and M. Aeschlimann, Spin-orbit enhanced demagnetization rate in Co/Pt-multilayers, *Appl. Phys. Lett.* **105**, 202402 (2014).
- [38] K. V. Shanavas, Z. S. Popović, and S. Satpathy, Theoretical model for Rashba spin-orbit interaction in D electrons, *Phys. Rev. B* **90**, 165108 (2014).
- [39] E. Carpena, H. Hedayat, F. Boschini, and C. Dallera, Ultrafast demagnetization of metals: Collapsed exchange versus collective excitations, *Phys. Rev. B* **91**, 174414 (2015).
- [40] E. Turgut, D. Zusin, D. Legut, K. Carva, R. Knut, J. M. Shaw, C. Chen, Z. Tao, H. T. Nembach, T. J. Silva, S. Mathias, M. Aeschlimann, P. M. Oppeneer, H. C. Kapteyn, M. M. Murnane,

- and P. Grychtol, Stoner versus Heisenberg: Ultrafast exchange reduction and magnon generation during laser-induced demagnetization, *Phys. Rev. B* **94**, 220408(R) (2016).
- [41] S. Eich, M. Plötzing, M. Rollinger, S. Emmerich, R. Adam, C. Chen, H. Cornelius Kapteyn, M. Murnane, L. Plucinski, D. Steil, B. Stadtmüller, M. Cinchetti, M. Aeschlimann, C. Schneider, and S. Mathias, Band structure evolution during the ultrafast ferromagnetic-paramagnetic phase transition in cobalt, *Sci. Adv.* **3**, e1602094 (2017).
- [42] R. Gort, K. Bühlmann, S. Däster, G. Salvatella, N. Hartmann, Y. Zemp, S. Hohenstein, C. Stieger, A. Fognini, T. Michlmayr, T. Bähler, A. Vaterlaus, and Y. Acremann, Early Stages of Ultrafast Spin Dynamics in a 3D Ferromagnet, *Phys. Rev. Lett.* **121**, 087206 (2018).
- [43] D. Zusin, P. M. Tengdin, M. Gopalakrishnan, C. Gentry, A. Blonsky, M. Gerrity, D. Legut, J. M. Shaw, H. T. Nembach, T. J. Silva, P. M. Oppeneer, H. C. Kapteyn, and M. M. Murnane, Direct measurement of the static and transient magneto-optical permittivity of cobalt across the entire M-edge in reflection geometry by use of polarization scanning, *Phys. Rev. B* **97**, 024433 (2018).
- [44] D. J. Higley, A. H. Reid, Z. Chen, L. L. Guyader, O. Hellwig, A. A. Lutman, T. Liu, P. Shafer, T. Chase, G. L. Dakovski, A. Mitra, E. Yuan, J. Schlappa, H. A. Dürr, W. F. Schlotter, and J. Stöhr, Femtosecond x-ray induced changes of the electronic and magnetic response of solids from electron redistribution, *Nat. Commun.* **10**, 5289 (2019).
- [45] M. Hennecke, D. Schick, T. Sidiropoulos, F. Willems, A. Heilmann, M. Bock, L. Ehrentraut, D. Engel, P. Hessian, B. Pfau, M. Schmidbauer, A. Furchner, M. Schnuerer, C. von Korff Schmising, and S. Eisebitt, Ultrafast element- and depth-resolved magnetization dynamics probed by transverse magneto-optical Kerr effect spectroscopy in the soft x-ray range, *Phys. Rev. Res.* **4**, L022062 (2022).